1

Introduction

1.1 Personalized Biomedical Diagnosis

1.1.1 Personalized Diagnosis

The world's older population continues to grow at an unprecedented rate. The proportion of people aged 60 years and over grows faster than any other age group, as shown in Figure 1.1 [1]. According to the expectation of the World Health Organization [2], between 2000 and 2050, the world's population of over 60 years of age will double from about 11% to 22%, and the absolute number of such people will also increase from 605 million to 2 billion. Among the aging countries, the most dramatic changes are now taking place in low and middle income countries with limited biomedical infrastructure, incomplete healthcare systems, and shortage of funds and resources. The current aging society also comes with special healthcare challenges due to limited hospital resources, doctors and related facilities. A portable and low-cost biomedical diagnosis instrument is thereby in high demand to meet the needs of the growing aging population in the form of personalized biomedical diagnosis.

Over the past several decades, biomedical diagnostic techniques such as the microscope [3], ultrasound [4–6], flow cytometry [7–9], and genetic sequencing [10–12], have improved the accurate monitoring of existing diseases, and also the understanding of the underlying causes of those diseases. However, to obtain highly sensitive measurements, current diagnosis instrument systems are usually bulky and expensive, their complicated operation requiring professional personnel. As such, they are usually only available in established hospitals or clinics, and hence are not flexible for multiple functionality diagnoses for on-site personalized diagnosis. These problems pose significant challenges for the personalized healthcare of aging populations, especially in low-income developing countries. As such, portable and affordable biomedical instruments that can be miniaturized are required to provide a point-of-care (POC) diagnosis [13–15].

A POC biomedical instrument is meant to perform the diagnosis at the site of patient care by a clinician or by the patient without the need for clinical laboratory facilities. The tests are rapid, portable, non-invasive, and easy-to-use, with timely testing results, which allow rapid clinical decision-making and also mitigate treatment delay. The development of these POC diagnostic and monitoring instruments

CMOS Integrated Lab-on-a-Chip System for Personalized Biomedical Diagnosis,
First Edition. Hao Yu, Mei Yan, and Xiwei Huang.

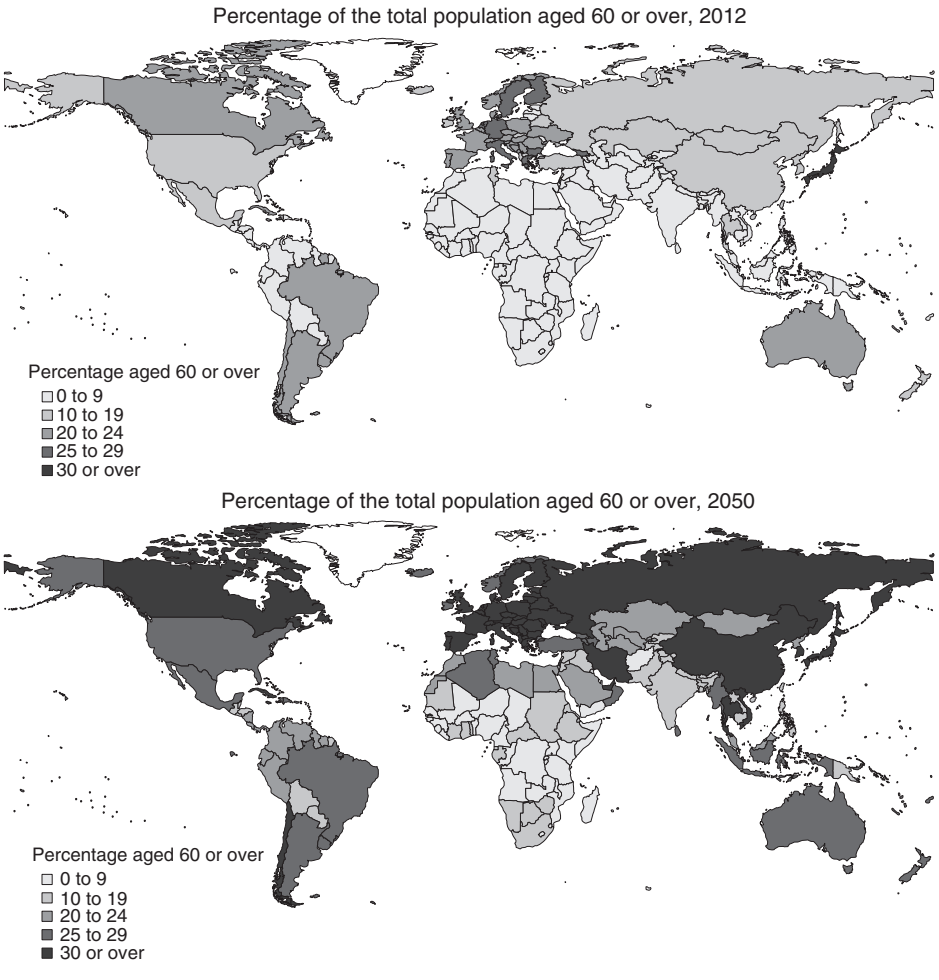

Figure 1.1 Global aging trends for the percentage of the total population at 60 years of age or over in 2012 and 2050 [1].

thereby allow individuals, especially these older people, to monitor their own health. It leads to a paradigm shift from conventional curative medicine, to predictive and personalized diagnostics [16]. Moreover, because factors such as medication adherence, genetics, age, nutrition, health, and environmental exposure can vary, and also the extent of biomedical treatment and drug response of each individual, people are becoming more interested in exploring the biology of the disease and its treatment at his or her own individual level. For example, people can use the information about his or her own genes, proteins, metabolites, etc. at the molecular level, and the leverage with the existing environment to prevent, diagnose, and treat the disease at the individual level. Therefore, such personalized biomedical diagnostics, with the existing supporting instrument platform, has emerged as a significant need for the coming aging world.

1.1.2 Conventional Biomedical Diagnostic Instruments

In the following section, three of the most widely-used traditional biomedical diagnosis instruments, namely the high-resolution optical microscope, flow cytometer, and DNA sequencer, are discussed as the starting point for comparison.

1.1.2.1 Optical Microscope

A microscope is an optical instrument that produces a magnified image of the biomedical object under inspection, compared with what the naked human eye can observe, using visible light with lenses. The optical microscope was invented more than 400 years ago by two Dutch spectacle makers, Hans and Zaccharias Janssen, then improved by Galileo and Antonie van Leeuwenhoek, and is the leading high-resolution visualization tool and the gold standard for biomedical imaging at the cellular level [17].

To achieve micrometer or sub-micrometer resolution, almost all microscopes require precise and expensive optical lenses, as well as a large distance between the object lens and eyepiece lens for the light to travel and reshape, as shown in Figure 1.2. The object to be observed is illuminated by a light source. As light passes through the object, the objective lens (i.e. the lens closest to the object) produces the corresponding magnified object image in the primary image angle. The eyepiece (i.e. the lens that people look into) acts as a magnifier that produces an enlarged image by the objective lens. The overall magnification of the microscope system is the

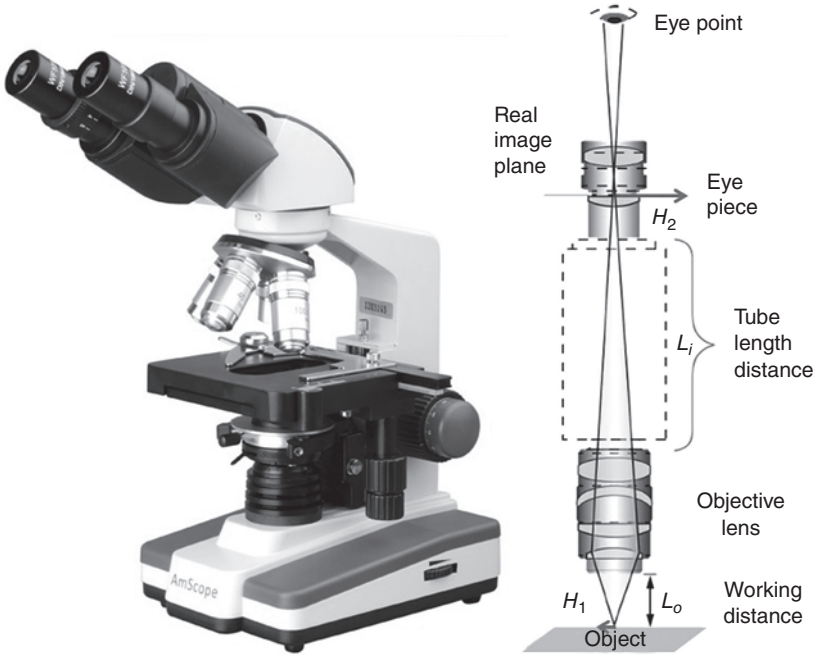

Figure 1.2 A typical microscope and its optical path with objective lens and eye piece. To reach high-resolution imaging capability, bulky, expensive, and sophisticated lenses are required.

multiplication of both the object and the eyepiece. The principle of magnification is based on the thin lens approximation as follows:

$$\frac{1}{L_i}+\frac{1}{L_o}=\frac{1}{F}M=\frac{L_i}{L_o}=\frac{H_2}{H_1} \tag{1.1}$$

where L_i and L_o are the image distance and object distance, F is the focal length of the objective lens, M is the magnification factor of the objective lens, and H_1 and H_2 are the sizes of object and image respectively. Therefore, a significant space L_i is usually required to produce a large microscopic magnification, which is the main difficulty for the minimization of the optical microscope.

Compared with the earliest compound microscope, the current design has evolved to incorporate multiple lenses, filters, polarizers, beam-splitters, sensors, illumination sources, and a host of other components, aimed at improving resolution and sample contrast. However, this basic microscope design has undergone very few fundamental changes over the centuries, so it bulky, expensive, and complicated, hence not suitable for the desired POC diagnosis.

1.1.2.2 Flow Cytometer

Flow cytometer is another widely-used biomedical instrument for applications in, for example, blood cell counting and sorting. Based on basic working principles, there are two types of flow cytometry methods, optical-based and electrochemical-based, as shown in Figure 1.3. With the help of sheath fluid and fluid dynamics effects, the blood cells are injected and passed through the measuring tunnel one at a time. For the optical-based cytometry shown in Figure 1.3(a), each cell along the path interacts with the laser beam respectively and the light intensity of the scattering is measured by the forward and orthogonal optical detectors. The measurement results depend on the size of the cell and its internal complexity, which can be used for cell differentiation and counting. Whereas, for the electrochemical based cytometry shown in Figure 1.3(b), pairs of electrodes are placed on both sides of a narrow orifice and a low-frequency

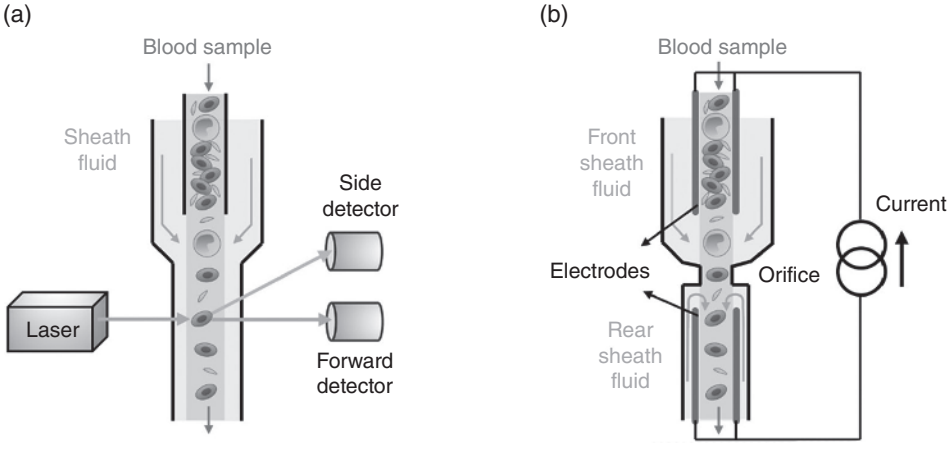

Figure 1.3 Diagrams of: (a) Optical-based; and (b) Electrochemical-based flow cytometry.

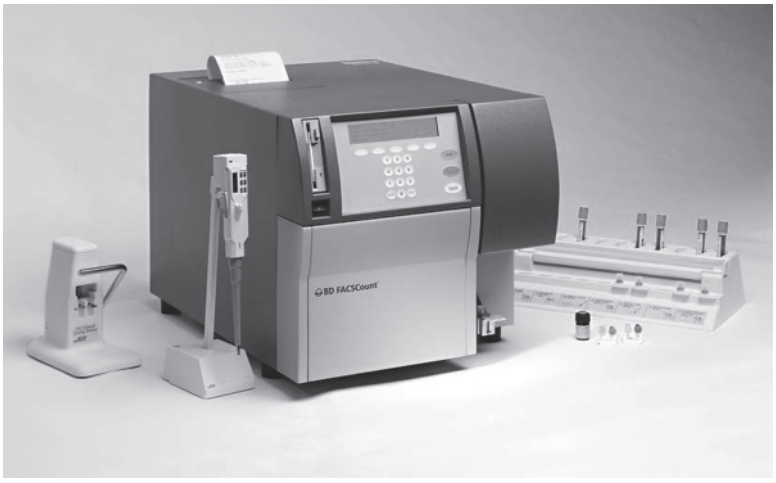

Figure 1.4 BD FACSCount™ cell cytometer system.

current is applied. When blood cells are driven through, the impedance values are measured, which vary with the cell size and composition.

As an example, the FACSCount, as shown in Figure 1.4, is one commercial optical-based flow cytometer system that can provide absolute and percentage counting results of various types of cells, such as red blood cells (RBCs), leukocytes, and CD4 T-lymphocytes. Clinicians rely on this system to diagnose the stage progression of HIV/AIDS, guide the treatment decision for HIV-infected persons, and evaluate the effectiveness of Antiretroviral Therapy (ART) [18]. However, it is only available in laboratory settings due to the limitations of bulky desktop size, prohibitive equipment cost ($27,000), high maintenance and reagent costs ($5–$20), low throughput (30–50 samples/day), and the need for an experienced operator, etc. [19]. Thus, it cannot meet the needs of personalized diagnosis.

1.1.2.3 DNA Sequencer

DNA sequencing, which detects the nucleotide order in DNA strands, enables the study of metagenomics and genetic disorders for diseases in aging people on an individual basis. Therefore, it plays an important role in personalized diagnostics. The first widely-applied DNA sequencing technique was the Sanger sequencing in the 1970s. This technique employs DNA polymerase to synthesize double-stranded DNA (dsDNA) from a primed single-stranded DNA (ssDNA) template. Four standard deoxyribonucleoside triphosphates (dNTPs), adenine (A), cytosine (C), guanine (G), and thymine (T), are used to extend the DNA, whereas four radioactively labeled di-dNTP (ddNTP) elements (ddATP, ddGTP, ddCTP, and ddTTP) are used to cease DNA extension. That is, once a ddNTP is attached to the DNA template, polymerase synthesis of this strand is invalid and no more dNTPs (or ddNTPs) can be added.

During sequencing, four chambers are employed for DNA synthesis. Each chamber is loaded with ssDNA templates, primers, polymerases, all four dNTPs, and one type of ddNTPs respectively. With sufficient dNTPs and a certain volume of labeled

ddNTP, DNA extension is randomly stopped, thereby producing a set of dsDNAs of various lengths. Locations of terminating ddNTPs in all four chambers can be visualized with electrophoresis gel. Since ddNTP in each location is complementary to the nucleotide in the template, the DNA sequence can be obtained after combining all the ddNTP types and location information. Sanger's contribution accelerated the process of DNA sequencing from roughly 10 base pairs (bp) per year to about 100 bp/day [20]. Later, the adoption of fluorescent labeling [21] and its associated optical detection hardware further improved Sanger's sequencing efficiency. In this technique, polymerase synthesis can be finished in one chamber by using four types of fluorescent labels. With the help of an optical detection system, each type of labeled ddNTP terminator can be identified based on the different color or wavelength they emit. These improvements have greatly helped the automation of the DNA sequencing process.

Since 2005, the next-generation sequencing (NGS) techniques substantially advanced the sequencing methods, targeting high-throughput and low-cost sequencing. A typical NGS machine is shown in Figure 1.5. Important examples of NGS technologies include the Solexa/Illumina bridge amplification method, which dominates this field currently [22], as well as Roche's pyrosequencing method [23] with bead-emulsified polymerase chain reaction (PCR) [24]. However, most of these methods require bulky and expensive optical instruments, which greatly restrict their use at the patient scale, such that only hospitals and research centers can afford them. In order to reduce the cost and size, new technologies targeted at personalized sequencing should be explored.

Figure 1.5 A typical optical DNA sequencer.

1.2 CMOS Sensor-based Lab-on-a-Chip for System Miniaturization

1.2.1 CMOS Sensor-based Lab-on-a-Chip

For bio-instrument miniaturization towards personalized diagnosis, effective solutions can only be derived from technologies that can resolve the scaling. One proved technology from the semiconductor industry is based on the complimentary metal-oxide semiconductor (CMOS) process. CMOS technology has been utilized in digital, analog, and mixed-signal integration circuits (ICs), such as microcontrollers, microprocessors, cell-phones, amplifiers, data converters, and transceivers, etc. More recently, the CMOS process has been developed in optical sensing, charge detection, temperature measurement, and electrochemical sensing applications, which can be realized by integrating readout circuits with on-chip sensing devices, such as photodiodes, ion-selected field effect transistors (ISFET), and microelectrodes. The main advantages of CMOS are the scalability in integration but also the variability in sensing. Large numbers or multiple functions of sensing devices (also called multi-modal sensors) can be integrated on one chip, so as to create mass-produced, low-cost, diversified, and miniaturized biomedical sensors for personalized diagnosis.

In most applications, biomedical samples are prepared and detected in an aqueous environment, which means that sensors usually need to be physically interfaced with fluidic samples, so as to realize a portable size. Thus, the emerging Lab-on-a-Chip (LOC) technique can combine a microfluidic system with the CMOS sensor. A microfluidic structure directs fluid samples towards the sensing sites, which are then detected by the underlying CMOS sensing devices. These devices, on the one hand, may act as voltage or current sources for actuating purpose. On the other hand, they may convert interesting biological information into an electric signal for sensing purposes.

As is implied by the name, Lab-on-a-Chip means a minimized chip-scale (a few square centimeters in size) device that has the ability to perform one or several laboratory functions [25–29]. Since LOCs need to deal with chemical or small biological objects, analyses in extremely small fluid volumes (microliters or even picoliters), it greatly relies on microfluidics for sample preparation, delivery, and on-chip processing. The recent advancement of LOC technology has provided a promising solution to integrate microfluidics [14], micro-electro-mechanical systems (MEMS), and CMOS multimodal sensors [30–33] on one platform, which allows a miniaturized biomedical sensing system without bulky mechanical components. For such a CMOS sensor-based LOC method, the reduced sample volume, portability, low cost, and the possibility to integrate multiple analytical devices, are key advantages over the traditional laboratory-scale instruments.

A diagram of the CMOS sensor-based LOC is shown in Figure 1.6. The sensor chip is fabricated through the standard CMOS process for the scaling benefit of low cost and mass production. It usually consists of a large amount (millions) of sensing nodes, or CMOS sensing pixels, to improve the sensing throughput. Thus, it can detect a great number of biological reactions simultaneously. In order to increase sensor density, the pixel design not only needs to consider the performance optimization, but also the scaling capability of continuously shrinking the pixel size. The CMOS sensor array can be further equipped with a fluidic package to carry and separate biomedical samples, so

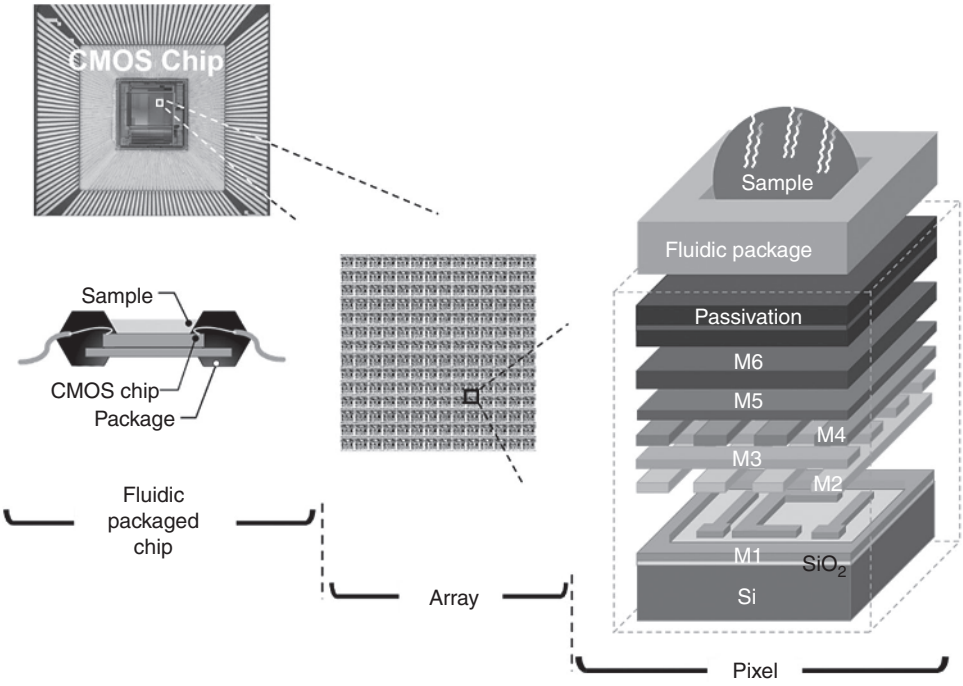

Figure 1.6 CMOS-based LOC integration for biomedical instrument miniaturization.

that a large volume of samples can be detected in parallel by their respective underlying pixels. After the sensor chip is fabricated, post processed, and packaged, it can be integrated with the microfluidic channel with fluidic packages to realize a completed LOC integration. Thus, such CMOS sensor-based LOC microsystems can create tremendous opportunities for future personalized diagnosis applications.

Building such CMOS-based LOC platforms can bring great potential and opportunities. It enables the development of multimodal CMOS sensors. The multimodal sensing types can vary from electrochemical, electric impedance, terahertz, and optical, etc., which will be mainly addressed in this book. Note that CMOS-based LOC platform can further integrate the data analytics part as well.

1.2.2 CMOS Sensor

1.2.2.1 CMOS Process Fundamentals

CMOS circuit design was invented in 1963 by Frank Wanlass at Fairchild Semiconductors. In 1968, a group led by Albert Medwin at RCA invented the first commercial CMOS integrated circuits that consist of 4000 series of CMOS logic gates. During the 1970s, CMOS technology was used in computing processor development, which led to the explosive growth of personal computers. It is estimated that the CMOS transistor is the most manufactured device in the history of mankind. Now, more than 95% of integrated circuits are fabricated in CMOS. One important reason behind this dominance is that CMOS is scalable for system integration.

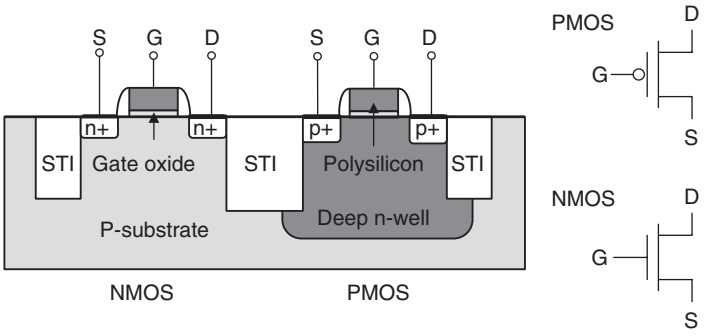

Figure 1.7 Cross-section view (left) and symbol (right) of CMOS technology components: NMOS and PMOS.

A metal oxide semiconductor (MOS) technology can be classified as PMOS (P-type MOS), NMOS (N-type MOS), and CMOS (Complementary MOS). The basic physical structure of MOS devices consists of a semiconductor, oxide, and a metal gate. Nowadays, polysilicon is more widely used as the gate (G). Voltage applied to the gate controls the current between source (S) and drain (D). Since very low power is consumed, MOS allows very high integration.

Figure 1.7 shows the components of a modern CMOS technology. Basically, it includes NMOS and PMOS transistors on the same substrate. For NMOS, the first letter "N" indicates the kind of carrier that carries the current flow between source and drain when the threshold voltage is reached. Thus, NMOS stands for transistors where negatively charged electrons are the current carriers between source and drain. PMOS stands for transistors where positively charged holes are the current carriers. The CMOS circuit uses both NMOS and PMOS transistors for pulling down to ground and up to power supply. The transistors are arranged in a structure formed by two complementary networks, Pull Up Network (PUN) and Pull Down Network (PDN). PUN is a network composed of PMOS transistors between output and power source, whereas PDN is an NMOS-type network between output and ground. Typically, in the CMOS circuit, only one of PUN and PDN is switched on and the other one is switched off with the corresponding gate capacitor to hold the charge information. This physical basic can be utilized in sensing.

CMOS technology requires fabrication of two different transistors – NMOS and PMOS on a single chip substrate. Actually, NMOS and PMOS need substrates with different kinds of doping in one integrated circuit. A silicon wafer always has one doping type and doping level. Hence, to accommodate both NMOS and PMOS transistors, CMOS technology requires creation of special regions, called wells, by impurity implantation in the substrate. The semiconductor type in these regions is opposite to the base substrate type. A p-well is created in an n-type substrate or, alternatively, an n-well is created in a p-type substrate. Thus, if the base substrate is p-type, the NMOS transistor is created in the p-type substrate, while the PMOS transistor is created in the n-well built into the p-type base substrate.

Historically, fabrication started with p-well technology, but now has completely shifted to n-well technology. This is due to the lower sheet resistance of the n-well

compared with the p-well, as electrons are more mobile than holes. The simplified n-well process to fabricate CMOS integrated circuits on a p-type silicon substrate works as follows. First, n-well regions are created for PMOS transistors by impurity implantation into the substrate. Next, a thick oxide (Shallow Trench Isolation, STI) surrounding the NMOS and PMOS active regions is grown to isolate each transistor. A thin gate oxide layer is then grown on the surface through thermal oxidation. After this process, n+ and p+ regions (source, drain, and channel-stop implants) are created. Finally, the metallization step creates metal interconnections in this process.

As each processing step requires that certain areas are defined on the chip by appropriate masks, the CMOS integrated circuit can be viewed as a set of patterned layers of doped silicon, polysilicon, metal, and insulating silicon dioxide. A layer is patterned before the next layer of material is applied on the chip. The lithography process is used to transfer a pattern onto a layer, which should be repeated for every layer using a different mask, since each layer has its own distinct requirements.

The main processing steps to fabricate an n-channel MOS transistor on a p-type silicon substrate are as follows. First, the oxidation of the silicon substrate (Figure 1.8(a)) is performed, which creates a relatively thick silicon dioxide layer on the surface, that is, the field oxide (Figure 1.8(b)). The field oxide is then selectively etched to expose the silicon surface on which the transistor will be created (Figure 1.8(c)). Then the surface is covered with a thin, high-quality oxide layer to form the gate oxide of the MOS transistor (Figure 1.8(d)). A polysilicon layer is then deposited onto the thin oxide (Figure 1.8(e)), which is used as both a gate material for MOS transistors as well as an interconnect medium in silicon. The resistivity of polysilicon, which is usually high, is reduced by doping it with impure atoms. Next, the polysilicon layer is patterned and etched to form the MOS transistor gate (Figure 1.8(f)). The thin gate oxide not masked by the polysilicon is also etched away, exposing the bare silicon surface. The drain and source junctions are to be formed, as in Figure 1.8(g).

Diffusion or ion implantation is used to dope the entire silicon surface with a high concentration of impurities (in this case donor atoms to produce n-type doping). Figure 1.8(h) shows two n-type regions (source and drain junctions) in the p-type substrate as doping penetrates the exposed areas of the silicon surface. The penetration of impurity doping into the polysilicon reduces its resistivity. After this stage, the entire surface is again covered with an insulating layer of silicon dioxide after the source and drain regions are completed (Figure 1.8(i)). Then contact windows for the source and drain are patterned into the oxide layer (Figure 1.8(j)). Interconnections are formed by evaporating the metal layer (aluminum/copper) onto the surface (Figure 1.8(k)), which is followed by patterning and etching of the metal layer (Figure 1.8(l)). A second or third layer of metallic interconnections can also be added after adding another oxide layer, by cutting (via) holes, depositing, and patterning the metal.

1.2.2.2 CMOS Sensor Technology

The development of CMOS technology offers the advantage of cost-effective CMOS integrated sensors, and the CMOS process can be applied to realize various CMOS sensors integrated for personalized diagnosis systems. Over the past few decades, many CMOS-based sensors have been developed for analyzing biological or chemical samples. Unlike conventional biomedical diagnostic instruments, new CMOS-compatible

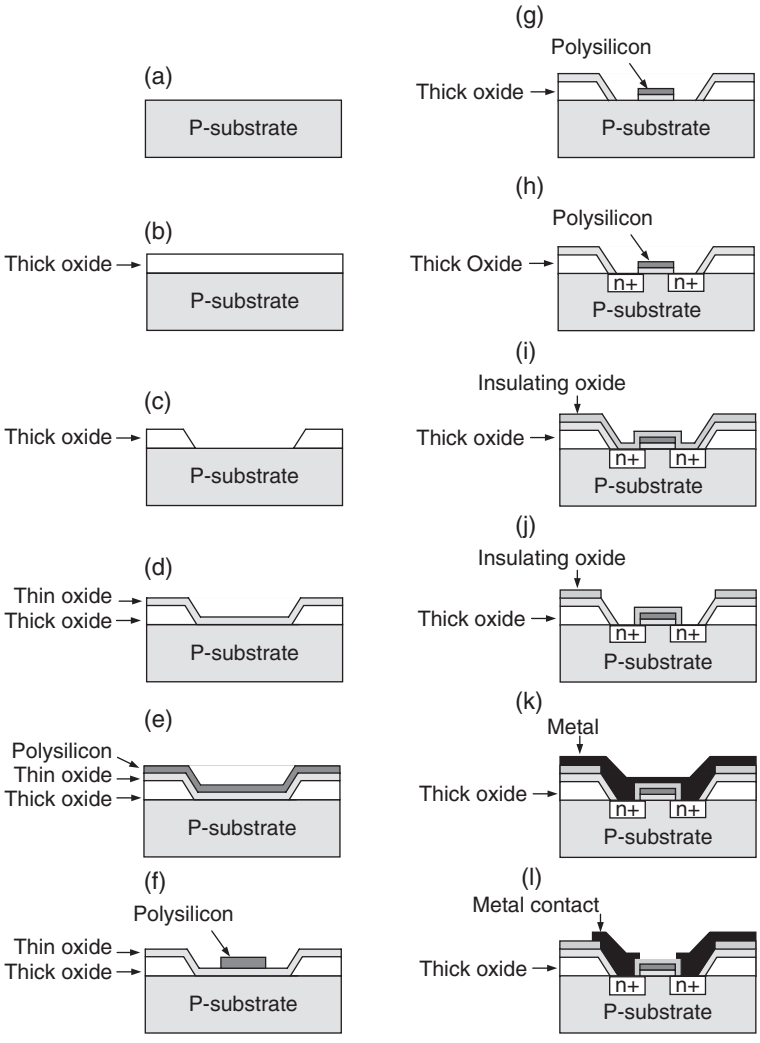

Figure 1.8 Process flow for the fabrication of an n-type MOSFET on p-type silicon.

biochemical sensing methods should be developed, especially for the conversion of biochemical information to circuit understandable languages, such as impedance, voltage, and current. For the CMOS process, the major materials involved are semiconductor materials (e.g. Si, SiO_2, and Si_3N_4) and metalic materials (e.g. Cu and Al); major manufacturing methods are doping, etching, deposition, and photolithography; and major fabricated structures are p-n junction, bipolar, and MOSFET. Thus, new CMOS-sensor-based biomedical sensing methods should evolve from these existing materials, processes, or structures to perform the biochemical-to-electrical conversion. One method is to directly fabricate the biochemical sensing part in standard CMOS processes. Another method is to first fabricate electrical-readout interfaces in standard CMOS processes and then use special surface treatments or post processing to make the biochemical sensing parts.

On the other hand, even though most of existing biomedical diagnostic methods vary, from either the substances used or procedures involved, the basic working principle can be categorized as optical-based and electrochemical-based. For the optical method, one way is to directly capture images to obtain the samples' physical properties such as shape, structure, or density. Another way is to first label or dye the samples and then detect the luminous parts to determine whether the desired reactions have occurred or not. Apart from optical characteristics, each object has its own electrical features that can be represented by impedance, voltage, or current. For the electrochemical method, one way is to directly measure these electrical properties of the target samples. Another way is to monitor the changing environmental conditions due to the samples' reactions or activities. New techniques can also be evolved from these two basic methods.

As examples, three types of CMOS process compatible biochemical sensing structures are illustrated. As shown in Figure 1.9(a), the p-n junction structure is utilized as a photodiode where photons are absorbed and converted into photocurrent. With illumination from the top, light intensity changes caused by the biomedical sample's optical properties are captured by the photodiode. This is a common optical sensing method utilizing a CMOS image sensor. In addition, electrochemical sensing structures are also involved, such as the voltage sensing in Figure 1.9(b) and current/impedance sensing in Figure 1.9(c). The electrode/electrode pair is normally employed to provide a steady biasing environment. Biochemical information will be converted into voltage or current signals that can be observed by CMOS sensors. In Figure 1.9(b), the non-conductive passivation layer (Si_3N_4) works as a sensing membrane. Ion density changes in the sample solution will charge or discharge the membrane. The resulting voltage shifts are detected by CMOS devices, whereas in Figure 1.9(c), an on-chip metal electrode will be fabricated, which forms an electrode pair together with the one in the sample solution. After applying a voltage drop, the current will flow through the electrode. The ion current value depends on the combined effects of sample and background solutions with varying resistance and capacitance. The induced current signals will also be detected by the underlying CMOS devices.

For CMOS sensors, large pixel arrays are preferred to reduce chip cost while improving the throughput, so that the capability to form a large pixel array and detect in parallel are the key issues to be addressed. Apart from the biochemical sensing part, other

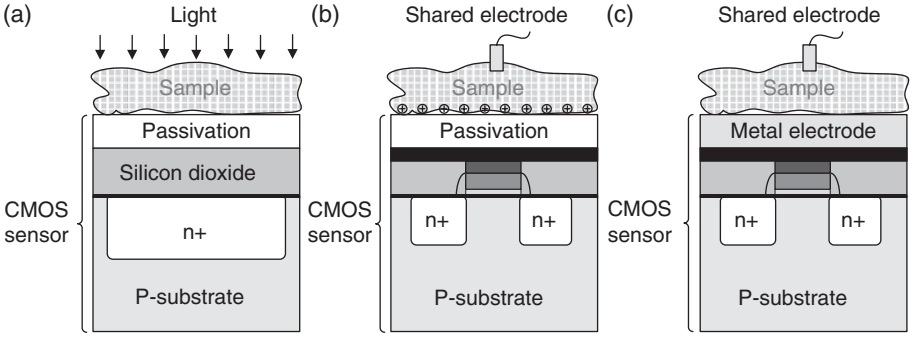

Figure 1.9 Diagrams of biochemical sensing structures; the sensing parts are: (a) p-n junction; (b) Passivation; and (c) Metal electrode pair.

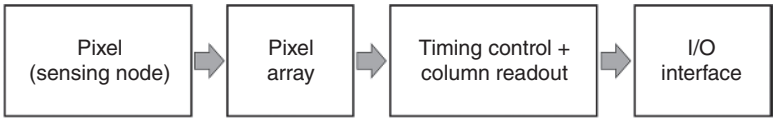

Figure 1.10 A typical architecture diagram of a CMOS sensor.

function blocks should also be involved to read out the converted signals or perform data processing. A typical CMOS sensor architecture is shown in Figure 1.10. The biomedical-to-electrical conversion is conducted in each pixel cell. A large amount of pixels can be arranged in a 2-D and pixel array. The pixel array is operated by timing control blocks and pixel signals are read out or processed by column readout blocks. All communication behaviors between the CMOS sensor and peripheral instruments, such as the voltage source or computer, are through the input/output (I/O) interface on chip.

In the following chapters, we will introduce impedance, terahertz, ultrasonic, MEMS, optical, or electrochemical sensors, etc. The CMOS impedance sensor employs an electrode array on top of the pixel array. It detects the sample's change in impedance magnitude and phase, which can be applied for single-cell detection. The CMOS Terahertz sensor can be applied as a THz spectroscopy for *in-vitro* tissue diagnosis. The CMOS ultrasound sensor can act as the front-end signal conditioner after the ultrasonic transducer for signal transmitting and receiving. The CMOS MEMS sensor can integrate the CMOS readout chip with the MEMS accelerometer to realize data fusion in a low-cost chip size fashion. The CMOS optical image sensor can capture images using a 2-D large pixel array to reach high resolution towards cell counting applications. The CMOS electrochemical sensor, or the CMOS pH sensor, can employ potentiometric ISFET pixels to sense the ion changes for bacteria detection or DNA sequencing application. In addition, the CMOS fabrication technology makes it possible to implement multimodal sensors that integrate multiple biomedical sensing modalities in one sensor chip, such as optical-electrochemical sensor or optical-energy harvesting sensor. In this case, high accuracy and diversified measurement can be realized when further fusing and recovering data from multimodal domains.

1.2.2.3 Multimodal CMOS Sensor

In biomedical testing, some properties of a reaction or biological material can be detected optically but not chemically, and vice versa for other properties. In some cases, it is only when these properties are known together that we can draw conclusions about the state of the reaction or biological material. The field of sensor fusion has received much attention recently as the combining of sensors can improve sensing capability. Thus, multimodal CMOS image sensors are required.

Light and electricity are two important media used in the measurement or control of biological samples such as proteins, neural cells, and DNA. Conventionally, optical imaging is based on microscopy technology, and electrical sensing of neural activity is through micro-electrode technology. In [34] or [35], a dual-mode CMOS image sensor is demonstrated. It can simultaneously capture optical and potential/electrochemical images of targeted biomedical samples, such as DNA or neural cells. As shown in Figure 1.11, the pixel array is composed of optical sensing pixels and potential sensing pixels that are interleaved. These two different types of pixels share the same timing and

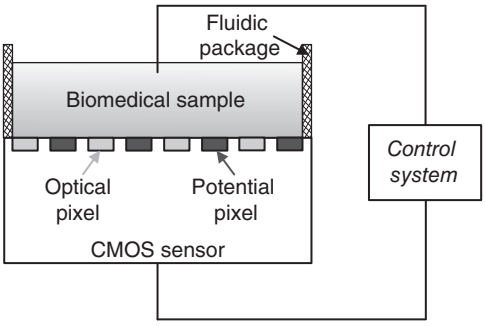

Figure 1.11 The concept of the optical and potential dual-mode CMOS image sensor.

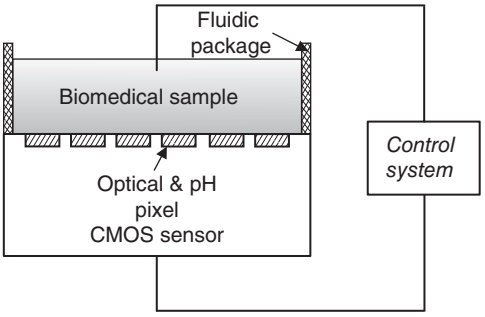

Figure 1.12 Schematic of the multimodal optical and pH CMOS image sensor.

column readout circuits, communication interface, package, and peripheral control system. In this way, system cost and size are minimized compared to the situation when these two sensor chips are separately fabricated.

For a CMOS sensor with a large pixel array, a small change in pixel size will make a large difference to the whole sensor chip. Thus, another attractive structure is to integrate multiple biochemical sensing devices into one pixel. Compared with the separately placed pixels in Figure 1.11, the pixel-level readout circuit can be shared by different types of sensing modes. In this way, chip size and cost can be further reduced. For example, in [36], a multimodal CMOS image sensor for pH and light sensing in real time is proposed. A photo sensor and a pH sensor are fused in the same pixel, as shown in Figure 1.12, enabling the optical and pH signals to be detected simultaneously in the same sensing area. As the pH sensing and optical sensing are built into the same area, more accurate chemical information can be extracted without loss of spatial resolution.

The fusion of various types of sensors has been receiving more attention recently, aiming to achieve high performance in the detection of signals from multiple domains. Next, more details about the LOC system components are introduced.

1.2.3 Microfluidics

1.2.3.1 Microfluidic Fundamentals

Microfluidics is a multidisciplinary engineering field where chemistry, physics, engineering, and biotechnology intersect to develop microscale chips, where the fluid analysis can

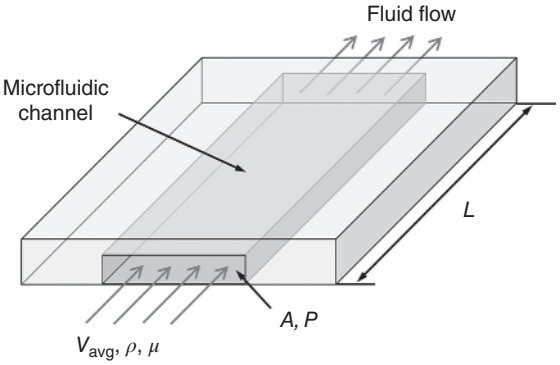

Figure 1.13 A typical microfluidic channel.

take place. The control and manipulation of the micro fluids are usually precisely and geometrically constrained to a microscale or nanoscale volume. For the typical microfluidic channel shown in Figure 1.13, the flow of the fluid can be characterized using the Reynolds number as follows:

$$Re = \frac{LV_{avg}\rho}{\mu} \tag{1.2}$$

where L is the most relevant channel length scale, V_{avg} is the average flow velocity, ρ is the fluid density, and μ is the fluid viscosity. For many microchannels, $L = 4A/P$, where A is the channel cross-sectional area, and P is the wetted channel perimeter. *Re* is usually much less than 100 (often < 1.0), due to the small dimensions of microchannels. In this *Re* regime, microfluidic flow is completely laminar without turbulence. Thus the micro sample can be transported in a relatively predictable manner through microchannels. When the *Re* increases to the range of 2000, the micro flow starts to change to a turbulent flow.

There are usually two methods of fluid actuation, namely electrokinetic flow and pressure driven flow. In electrokinetic flow, the fluids are driven by electroosmotic pumping. In pressure driven flow, the fluid is driven through the channel by positive displacement pumps such as syringe pumps. The advantage of electrokinetic flow over pressure driven flow is that it can couple other on-chip electronic applications. However, electrokinetic flow often requires very high voltages. Without off-chip power supplies, it is difficult to miniaturize. One other significant disadvantage of electrokinetic flow is the variability in surface properties. For example, the proteins absorbed into the channel walls can substantially change the surface charge characteristics, and hence lead to a change in fluid velocity. This problem will result in unpredictable and irregular long-term time dependency on the fluid flow

There is also another kind of microfluidics, droplet-based digital microfluidics. This employs electrowetting-on-dielectric to precisely manipulate discrete droplets of biochemical samples and reagents at microliter or picoliter volumes under digital clock control. It can combine electronics with biology, and integrate together a number of bioassay operations, such as sample preparation, separation, mixture, analysis, and detection to form a miniaturized digital microfluidic biochip (DMFB) and automate laboratory procedures in immunoassays, biochemistry, and molecular biology.

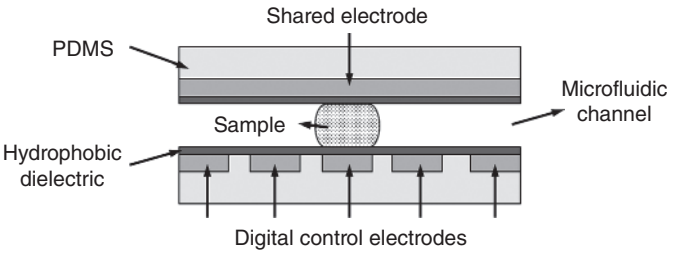

Figure 1.14 Cross-sectional schematic of a unit cell on digital microfluidic arrays.

An example of DMFB is shown in Figure 1.14. Compared to conventional expensive and cumbersome laboratory procedures, DMFBs show the advantages of lower cost, higher sensitivity, easier system integration, and less likelihood of human error.

There are several advantages of using microfluidic devices in clinically useful technologies to perform biomedical diagnosis:

1) Microfluidic technologies make it possible to fabricate highly integrated devices so that several different functions, such as blood or saliva filtering, desalting, denaturation, concentration, and derivatization, can be performed on the same chip.
2) Small volumes lead to fast analyses; moreover, the small amount of reagents and analytes used is especially important for expensive reagents.
3) Material cost is negligible in micro-systems. The techniques used to fabricate microfluidic devices are relatively inexpensive and suitable for highly multiplexed devices and mass production.

After the fundamentals of fluid flow and sample transportation becoming well developed, microfluidics has recently developed towards integrated devices that incorporate multiple fluidic, mechanical, and electronic components as well as various chemical processes onto a single chip. There has been a major push towards bio-imaging instrument miniaturization.

1.2.3.2 Microfluidics Fabrication

To fabricate microfluidic channels, polymers, instead of silicon and glass, are commonly used. Specifically, the poly-dimethylsiloxane (PDMS) is widely used as it is inexpensive, flexible, optically transparent, and biological compatible. The fabrication of microfluidic channels using the conventional soft-lithography process is presented here:

1) **Photolithography Mask**
   Some examples of the designed microfluidic channel masks are shown in Figure 1.15. First, the channel microstructures or features are designed in a computer-aided design (CAD) program, such as the AutoCAD (Autodesk, San Rafael, CA). Using commercial services, the CAD-generated patterns are printed onto a transparent photolithography mask. The photolithography mask is an opaque film or plate template with transparent areas that allow light to shine through in the designed pattern. The feature size (or the lateral resolution) of the mask is determined by its material; three types of base materials are commonly used to make photolithography masks, namely Quartz, Soda Lime (SL), and polyester film. Quartz and SL masks are high resolution, easy to clean, stable, but expensive. Polyester film masks have less resolution, but are low cost and much easier to handle.

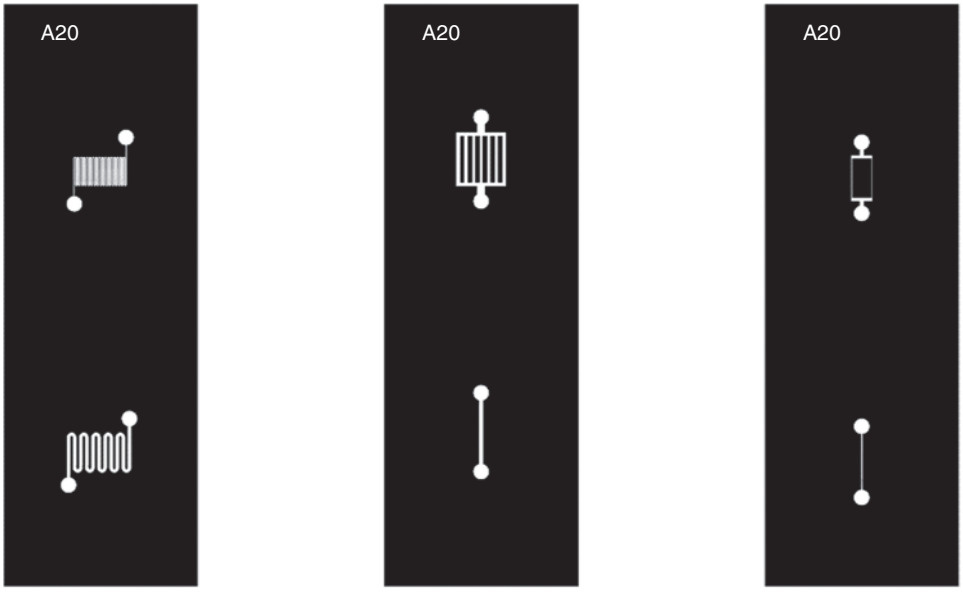

Figure 1.15 Microfluidic channel masks designed by AutoCAD.

2) **SU-8 Mold**

After the turnaround time, the designed masks are sent back for microfluidic channel mold fabrication. Here, the negative photoresist SU-8 (SU-8 25, Microchem, MA) is used, which is a high contrast and epoxy-based photoresist for micro-machining. The SU-8 has superb chemical and temperature resistance and can build a thickness from 1 to 200 μm with the single spin coat process. A normal process is shown in Figure 1.16:

1) *Substrate Pretreat*

Both a silicon wafer and glass slide can be used as the SU-8 substrate. Here we take the glass slide as an example due to its low cost. To obtain the maximum process reliability, substrates need to be clean and dry before applying the SU-8 resist. The glass slide is pretreated in the following way:

1) Soak and wash the glass slide with acetone for at least 1 h for solvent cleaning.
2) Use distilled water to rinse the glass slide, and then use a stream of air or nitrogen to blow to dry.
3) To dehydrate the surface, bake the cleaned glass slide at 200 °C for 5 min on a hotplate.
4) Plasma treat for 10 min to further clean and dehydrate the glass slide surface.

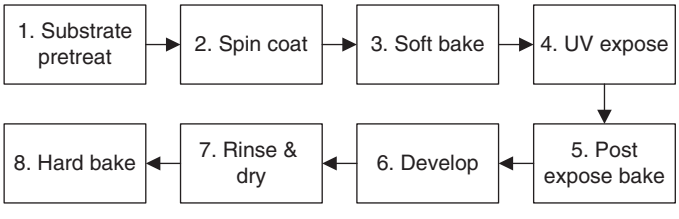

Figure 1.16 PDMS mold fabrication process.

2) *Spin Coat*
   Next, the SU-8 is spin-coated using a spin machine (SCS G3P-8, Indianapolis, IN) onto the clean glass slide. The spin speed directly determines the height of the mold, which is also the height of the final PDMS microfluidic channel. The detailed steps are:
   5) Pour SU-8 onto the glass slide (~10–15 ml per glass slide for static dispense), then degas in a vacuum oven for 1 h to remove air bubbles.
   6) Spin coat for thin film deposition; the spin speed needs to be set to correspond to different film heights.
3) *Soft Bake*
   After the photoresist is spin-coated onto the glass slide substrate, it should be soft-baked on a hot plate to evaporate the solvent as well as to densify the film. As the solvent evaporation rate is affected by the heat transfer and ventilation rate, baking times should be optimized for proximity and the convection oven bake process. The process is:
   7) Bake on a 65 °C hot plate for 5 min, then at 95 °C for 15 min.
4) *UV Exposure*
   The soft-baked glass slide with SU-8 film is exposed to UV. SU-8 is practically transparent and insensitive above 400 nm, but has high actinic absorption below 350 nm. The exposure dose also affects the film thickness. The process is:
   8) UV exposure of 200 mJ/cm^2 energy for 30 s.
5) *Post Expose Bake*
   Following exposure, post expose bake (PEB) needs to be performed to selectively cross-link the exposed portions of the film. This is realized through a two-step contact hot plate baking process, as indicated below:
   9) Post UV exposure bake on a 65 °C hot plate for 1 min, then at 95 °C for 4 min.
6) *Develop*
   After PEB, the SU-8 is developed using an SU-8 developer. The approximate developing time is 6 min, but it can vary widely as a function of temperature or agitation rate, i.e.:
   10) Develop the PEB glass slide using the SU-8 developer for 6 min.
7) *Rinse and Dry*
   Following the development, the substrate should be rinsed using isopropyl alcohol (IPA), and then dried under a gentle stream of air or nitrogen. It then undergoes a final hard bake. The detailed steps are:
   11) Rinse the substrate using IPA and dry.
   12) Bake the substrate on a 200 °C hot plate for 10 min.
   13) Cool the slides and place them into the culture dish.

3) **PDMS Replica**
   After the SU-8 mold is ready, we can cast the PDMS replica, that is, the microfluidic channel. The whole mask, mold, and PDMS channel fabrication process flow is shown in Figure 1.17.
   The steps are:
   a) Prepare the PDMS mixture for casting, a volumetric ratio of 10:1 mixture of PDMS (Sylgard 184, Dow Corning, MI) and curing agent, and pour into the SU-8 mold.

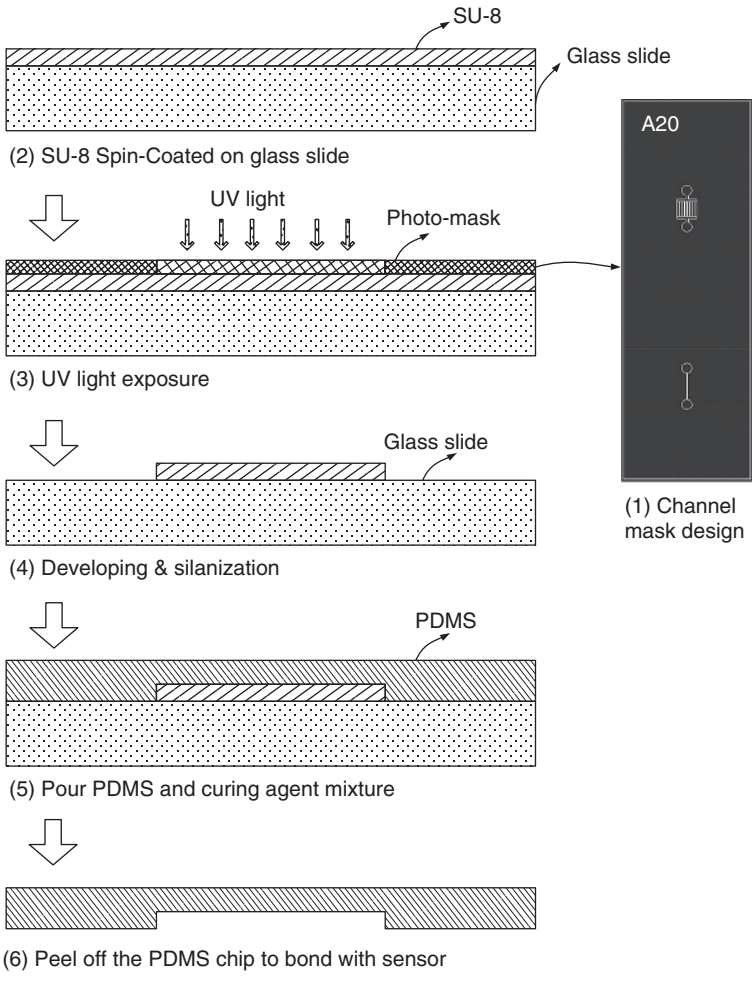

Figure 1.17 Microfluidic channel fabrication process using the soft lithography technique.

b) Degas for 1 h in a vacuum oven to remove any bubbles from the PDMS mixture.
c) Take out the glass slide and bake in the oven for 2 h.
d) After the PDMS replica becomes dry and hard, take out and prepare to cut the channel out and peel off from the glass substrate.
e) Use a puncher to punch holes in the top of the PDMS replica for inlet and outlet channels, which are to be connected with silastic laboratory tubes to a syringe pump and waste bin.
f) Use IPA and de-ionized (DI) water to rinse the PDMS channel. Dry the channel for the final bonding with the CMOS sensors.

Now, the PDMS microfluidic channel fabrication process is complete.

1.3 Objectives and Organization of this Book

1.3.1 Objectives

Towards the personalized diagnosis for the aging society, miniaturized bio-instrumentation is demanded. As such, the conventional bulky optical lens and other mechanical components can no longer be applied. We need to develop CMOS-based LOC integrated systems that integrate microfluidics, MEMS, and CMOS sensors, as well as smart data analysis for biomedical diagnosis. The standard CMOS process provides an low-cost system-on-chip (SOC) solution to integrate sensors from multimodal domains, which has raised many new design challenges, such as how to develop multimodal sensors for system integration; how to integrate with MEMS and microfluidic channels from a device technology perspective; as well as data fusing and smart processing of multiple domains from the system application perspective.

Therefore, in this book, we have particularly reported on the recent progress in the CMOS integrated LOC system for personalized diagnosis [38–61]. The CMOS sensors we developed for the LOC integrated biomedical diagnostic system include multiple modes, which are:

1) CMOS electronic impedance sensor for rare cell detection and counting;
2) CMOS Terahertz sensor for non-invasive imaging;
3) CMOS capacitive-micromachined-ultrasonic-transducer (CMUT) sensor for non-invasive 3-D ultrasound imaging;
4) CMOS ISFET sensor for ion imaging towards DNA sequencing application; and
5) CMOS optical sensor for microfluidic imaging towards cell detection, recognition, and counting applications.

We will illustrate the need and application of the five corresponding bio-imaging diagnosis methods, as well as design problems addressed when being miniaturized. In addition, for MEMS integration, we further present a 3-D CMOS MEMS integration method for high-throughput sensing data readout with smaller form factor, latency, and power consumption. Moreover, two dual-mode sensors are presented. One is from the sensing capability point of view, where the CMOS optical sensing and CMOS ion sensing are integrated together in the same sensing pixel for higher accuracy and lower noise diagnosis. The other is to tackle the problem of energy, where a CMOS image sensor with both energy harvesting mode and optical sensing mode is illustrated. Finally, the smart data analytics are integrated into the discussion of optical image sensor-based lensless cell counting applications.

Our thorough study to explore multimodal CMOS sensors in LOC for the portable personalized diagnosis system could pave the way towards a variety of personalized diagnosis applications. As a conclusion, the CMOS multimodal sensor-based LOC system has shown great potential in providing future personalized e-healthcare solution for the coming aging society.

1.3.2 Organization

The rest of the book is organized into three major parts. Chapters 2 to 7 discuss CMOS sensor design and several CMOS sensor technologies, namely CMOS electronic impedance

sensor, CMOS Terahertz sensor, CMUT ultrasound sensor, CMOS 3D-integrated MEMS sensor, and CMOS optical sensor for microfluidic contact imaging. The two dual-mode sensors are illustrated in Chapters 8 and 9, that is, dual-mode chemical/optical image sensor and dual-mode energy-harvesting image sensing. Finally, based on the aforementioned sensors, two important applications, DNA sequencing and cell counting, are elaborated upon. Chapter 10 focuses on DNA sequencing applications. Chapter 11 covers cell imaging and counting applications. Finally, Chapter 12 concludes the whole book.

References

1 WHO Global Brief for World Health Day (2012) Available at: http://www.who.int/ageing/publications/whd2012_global_brief/en/
2 WHO Ageing and Life Course. Available at: http://www.who.int/ageing/en/
3 T. Wilson (1990) *Confocal Microscopy*, vol. 426 Academic Press: London, pp. 1–64.
4 X. Huang, J.H. Cheong, H.-K. Cha, H. Yu, M. Je, and H. Yu (2013) A high-frequency transimpedance amplifier for CMOS integrated 2D CMUT array towards 3D ultrasound imaging. In: *International Conference of the IEEE Engineering in Medicine and Biology Society (EMBC)*, pp. 101–104.
5 I. Kim, H. Kim, F. Griggio, R.L. Tutwiler, T.N. Jackson, *et al*. (2009) CMOS ultrasound transceiver chip for high-resolution ultrasonic imaging systems. *IEEE Transactions on Biomedical Circuits and Systems (TBCAS)*, 3(5), 293–303.
6 G. Gurun, P. Hasler and F.L. Degertekin (2011) Front-end receiver electronics for high-frequency monolithic CMUT-on-CMOS imaging arrays. *IEEE Transactions on Ultrasonics, Ferroelectrics and Frequency Control (TUFFC)*, 58(8), 1658–1668.
7 H.M. Shapiro (2003) *Practical Flow Cytometry*, 4th edition. John Wiley & Sons.
8 A.L. Givan (2001) *Flow Cytometry: First Principles*, 2nd edition. John Wiley & Sons.
9 M. Brown and C. Wittwer, (2000) Flow cytometry: Principles and clinical applications in hematology. *Clinical Chemistry*, 46(8), 1221–1229.
10 J. Shendure and H. Ji (2008) Next-generation DNA sequencing. *Nature Biotechnology*, 26, 1135–1145.
11 M. Margulies, M. Egholm, W.E. Altman, S. Attiya, J.S. Bader, *et al*. (2005) Genome sequencing in microfabricated high-density picolitre reactors. *Nature*, 437, 376–380.
12 D.R. Bentley, S. Balasubramanian, H.P. Swerdlow, G.P. Smith, J. Milton, C.G. *et al*. (2008) Accurate whole human genome sequencing using reversible terminator chemistry. *Nature*, 456, 53–59.
13 G.J. Kost (2002) *Principles and Practice of Point-of-care Testing*. Lippincott Williams & Wilkins: Philadelphia.
14 S.K. Sia and L.J. Kricka (2008) Microfluidics and point-of-care testing. *Lab on a Chip*, 8(12), 1982–1983.
15 P. Yager, G.J. Domingo and J. Gerdes (2008) Point-of-care diagnostics for global health. *Annual Review of Biomedical Engineering*, 10, 107–144.
16 B. Korte (2010) *NIH Fact Sheet: Point-of-Care Diagnostic Testing*. https://report.nih.gov/NIHfactsheets/ViewFactSheet.aspx?csid=112.
17 C. Yang and D. Psaltis (2007) Building a Microscopic Microscope. *ENGenious*, 6, 44–47.

18 C.F. Gilks, S. Crowley, R. Ekpini, S. Gove, J. Perriens, *et al.* (2006) The WHO public-health approach to antiretroviral treatment against HIV in resource-limited settings. *The Lancet*, 368(9534), 505–510.

19 S.J. Moon, H.O. Keles, A. Ozcan, A. Khademhosseini, E. Hæggstrom, *et al.* (2009) Integrating microfluidics and lensless imaging for point-of-care testing. *Biosensors and Bioelectronics*, 24(11), 3208–3214.

20 L. Hartwell, L. Hood, M.L. Goldberg, A. Reynolds, L. Silver and R. Veres (2008) *Genetics: from Genes to Genomes*. McGraw-Hill: New York.

21 L.M. Smith, J.Z. Sanders, R.J. Kaiser, P. Hughes, C. Dodd, *et al.* (1986) Fluorescence detection in automated DNA sequence analysis. *Nature*, 321(6071), 674–679.

22 S. Balasubramanian (2003) Polynucleotide sequencing, Google Patents.

23 P. Nyren (2001) Method of sequencing DNA based on the detection of the release of pyrophosphate and enzymatic nucleotide degradation, Google Patents.

24 M. Margulies, M. Egholm, W.E. Altman, S. Attiya, J.S. Bader, *et al.* (2005) Genome sequencing in microfabricated high-density picolitre reactors. *Nature*, 437(7057), 376–380.

25 R. Daw and J. Finkelstein (2006) Lab on a chip. *Nature*, 442(7101), 367–367.

26 G.M. Whitesides (2006) The origins and the future of microfluidics. *Nature*, 442(7101), 368–373.

27 D. Mark, S. Haeberle, G. Roth, F. von Stetten and R. Zengerle (2010) Microfluidic lab-on-a-chip platforms: requirements, characteristics and applications. *Chemical Society Reviews*, 39(3), 1153–1182.

28 Y. Zhao, D. Chen, H. Yue, J.B. French, J. Rufo, *et al.* (2013) Lab-on-a-chip technologies for single-molecule studies. *Lab on a Chip*, 13(12), 2183–2198.

29 M. Medina-Sanchez, S. Miserere and A. Merkoci (2012) Nanomaterials and lab-on-a-chip technologies, *Lab on a Chip*, 12(11), 1932–1943.

30 Y.-S. Lin, D. Sylvester and D. Blaauw (2008) An ultra low power 1 V, 220 nW temperature sensor for passive wireless applications. In: *IEEE Custom Integrated Circuits Conference (CICC)*, pp. 507–510.

31 S. Hanson and D. Sylvester (2009) A 0.45–0.7 V sub-microwatt CMOS image sensor for ultra-low power applications. In: *IEEE Symposium on VLSI Circuits (VLSIC)*, pp. 176–177.

32 Y.-S. Lin, D.M. Sylvester and D.T. Blaauw (2009) A 150 pW program-and-hold timer for ultra-low-power sensor platforms. In: *IEEE International Solid-State Circuits Conference (ISSCC)*, pp. 326–327.

33 S. Hanson, Z. Foo, D. Blaauw and D. Sylvester (2010) A 0.5 V sub-microwatt CMOS image sensor with pulse-width modulation read-out. *IEEE Journal of Solid-State Circuits (JSSC)*, 45(4), 759–767.

34 T. Tokuda, A. Yamamoto, K. Kagawa, M. Nunoshita and J. Ohta (2006) A CMOS image sensor with optical and potential dual imaging function for on-chip bioscientific applications. *Sensors and Actuators A: Physical*, 125(2), 273–280.

35 T. Tokuda, K. Tanaka, M. Matsuo, K. Kagawa, M. Nunoshita and J. Ohta, (2007) Optical and electrochemical dual-image CMOS sensor for on-chip biomolecular sensing applications. *Sensors and Actuators A: Physical*, 135(2), 315–322.

36 J. Matsuo, K. Sawada, H. Takao and M. Ishida (2008) Multimodal pH and light imaging devices for dynamic chemical reaction observation. In: Proceedings of the μTAS, pp. 326–328.

37 M.P. McRae, G. Simmons, J. Wong and J.T. McDevitt (2016) Programmable bio-nanochip platform: A point-of-care biosensor system with the capacity to learn. *Accounts of Chemical Research*, 49(7), 1359–1368.

38 Y. Jiang, X. Liu, T.C. Dang, M. Yan, H. Yu, *et al*. (2016) A 512 × 576 65-nm CMOS ISFET sensor for food safety screening with 123.8 mV/pH sensitivity and 0.01 pH resolution. pp. 1–2.

39 Y. Jiang, X. Liu, X. Huang, Y. Shang, M. Yan and H. Yu (2016) Lab-on-CMOS: A multi-modal CMOS sensor platform towards personalized DNA sequencing. In: IEEE International Symposium on Circuits and Systems (ISCAS), pp. 2266–2269.

40 X. Huang, Y. Jiang, Y. Shang, H. Yu and L. Sun (2015) A CMOS THz-sensing system towards label-free DNA sequencing. In: IEEE 11th International Conference on ASIC (ASICON), I pp. 1–4.

41 Y. Jiang, X. Liu, X. Huang, J. Guo, M. Yan, *et al*. (2015) A 201 mV/pH, 375 fps and 512 × 576 CMOS ISFET sensor in 65 nm CMOS technology. In: IEEE Conference on Custom Integrated Circuits (CICC), pp. 1–4.

42 D. Jeon, Q. Dong, Y. Kim, X. Wang, S. Chen, *et al*. (2015) A 23 mW face recognition accelerator in 40 nm CMOS with mostly-read 5 T memory. In: VLSI Symposium on VLSI Circuits (VLSI Circuits), pp. C48–C49.

43 X. Liu, L. Yao, P. Li, M. Yan, S.-C. Yen, *et al*. (2015) A 16-channel 24-V 1.8-mA power efficiency enhanced neural/muscular stimulator with exponentially decaying stimulation current. In: IEEE International Symposium on Circuits and Systems (ISCAS), pp. 2992–2995.

44 Y. Shang, H. Yu, C. Yang, Y. Liang and W.M. Lim (2014) 239–281 GHz sub-THz imager with 100 MHz resolution by CMOS direct-conversion receiver with on-chip circular-polarized SIW antenna. In: IEEE Proceedings of the Custom Integrated Circuits Conference (CICC), pp. 1–4.

45 Y. Shang, H. Yu, C. Yang, S. Hu and M. Je (2014) A high-sensitivity 135 GHz millimeter-wave imager by differential transmission-line loaded split-ring resonator in 65 nm CMOS. In: 44th European Conferences on Solid State Device Research (ESSDERC), pp. 166–169.

46 S. Chua, A. Razzaq, K. Wee, K. Li, H. Yu and C. Tan (2014) 3D CMOS-MEMS stacking with TSV-less and face-to-face direct metal bonding. In: Symposium on VLSI Technology (VLSI-Technology): Digest of Technical Papers, pp. 1–2.

47 X. Huang, F. Wang, J. Guo, M. Yan, Y. Hao and K.S. Yeo (2014) A 64 × 64 1200 fps CMOS ion-image sensor with suppressed fixed-pattern noise for accurate high-throughput DNA sequencing. In: Symposium on VLSI Circuits Digest of Technical Papers, pp. 1–2.

48 S. Chua, A. Razzaq, K. Wee, K. Li, H. Yu and C.S. Tan (2014) TSV-less 3-D stacking of MEMS and CMOS via low temperature Al–Au direct bonding with simultaneous formation of hermetic seal. In: IEEE 64th Conference on Electronic Components and Technology Conference (ECTC), pp. 324–331.

49 R. Nadipalli, J. Fan, K. Li, K. Wee, H. Yu and C. Tan (2011) 3D integration of MEMS and CMOS via Cu–Cu bonding with simultaneous formation of electrical, mechanical and hermetic bonds. In: 2011 IEEE International Conference on 3D Systems Integration Conference (3DIC), pp. 1–5.

50 M. Yan, X. Huang, Q. Jia, R. Nadipalli, Y. Shang, *et al*. (2012) High-speed CMOS image sensor for high-throughput lensless microfluidic imaging system with point-of-care application. In; SPIE 8298, Sensors, Cameras, and Systems for Industrial and Scientific Applications XIII, 829804.

51 N. Li, H. Yu, C. Yang, Y. Shang, X. Li and X. Liu (2015) A high-sensitivity 135 GHz millimeter-wave imager by compact split-ring resonator in 65-nm CMOS. *Solid-State Electronics*, 113, 54–60.

52 X. Huang, H. Yu, X. Liu, Y. Jiang and M. Yan (2015) A single-frame superresolution algorithm for lab-on-a-chip lensless microfluidic imaging. *IEEE Design & Test*, 32(6), 32–40.

53 X. Huang, H. Yu, X. Liu, Y. Jiang, M. Yan and D. Wu (2015) A dual-mode large-arrayed CMOS ISFET sensor for accurate and high-throughput pH sensing in biomedical diagnosis. *IEEE Transactions on Biomedical Engineering*, 62(9), 2224–2233.

54 I. Cevik, X. Huang, H. Yu, M. Yan and S.U. Ay (2015) An ultra-low power CMOS image sensor with on-chip energy harvesting and power management capability. *Sensors*, 15(3), 5531–5554.

55 J. Guo, X. Huang, D. Shi, H. Yu, Y. Ai, *et al*. (2014) Portable resistive pulse-activated lens-free cell imaging system. *RSC Advances*, 4(99), 56342–56345.

56 Y. Shang, H. Yu, S. Hu, Y. Liang, X. Bi and M.A. Arasu (2014) High-sensitivity CMOS Super-regenerative receiver with quench-controlled high-Q metamaterial resonator for Millimeter-Wave Imaging at 96 and 135 GHz. *IEEE Transactions on Microwave Theory and Techniques*, 62(12), 3095–3106.

57 Y. Shang, H. Yu, H. Fu and W.M. Lim (2014) A 239–281 GHz CMOS receiver with on-chip circular-polarized substrate integrated waveguide antenna for sub-terahertz imaging. *IEEE Transactions on Terahertz Science and Technology*, 4(6), 686–695.

58 X. Huang, X. Wang, M. Yan and H. Yu (2015) A robust recognition error recovery for micro-flow cytometer by machine-learning enhanced single-frame super-resolution processing. *Integration, the VLSI Journal*, 51, 208–218.

59 X. Huang, J. Guo, X. Wang, M. Yan, Y. Kang and H. Yu (2014) A contact-imaging based microfluidic cytometer with machine-learning for single-frame super-resolution processing. *PloS one*, 9(8), e104539.

60 T.S. Pui, Y. Chen, C.C. Wong, R. Nadipalli, R. Weerasekera, *et al*. (2013) High density CMOS electrode array for high-throughput and automated cell counting. *Sensors and Actuators B: Chemical*, 181, 842–849.

61 Y. Chen, C.C. Wong, T.S. Pui, R. Nadipalli, R. Weerasekera, *et al*. (2012) CMOS high density electrical impedance biosensor array for tumor cell detection. *Sensors and Actuators B: Chemical*, 173, 903–907.